T2*-Weighted Echo-Planar Imaging of Inner Fields-of-View Using 2D-Selective RF Excitations

Jürgen Finsterbusch[1,2]

[1]*Department of Systems Neuroscience, University Medical Center Hamburg-Eppendorf, Hamburg, Germany,* [2]*Neuroimage Nord, University Medical Centers Hamburg-Kiel-Lübeck, Hamburg-Kiel-Lübeck, Germany*

With spatially 2D-selective RF (2DRF) excitations [1,2] rectangular profiles can be excited which can be used to acquire inner fields-of-view (FOV) without phase-encoding aliasing. Thus, geometric distortions in echo-planar imaging (EPI) that are caused by magnetic field and susceptibility inhomogeneities, can be reduced for small target regions [3]. The feasibility of this approach to acquire high-resolution echo-planar images of inner objects has been demonstrated for diffusion-weighted imaging of the spinal cord [4-6]. In this study, two of the developed setups [5,6] are applied to T2*-weighted imaging of the brain in order to improve the spatial resolution of EPI-based functional neuroimaging.

Methods

The basic setups used in the present study are sketched in Fig. 1. In the first ("FID"), a FID signal is acquired and the 2DRF excitation's line and blip directions coincides with the imaging slice and phase direction (Fig. 1a) which means that the unwanted side excitations appearing in the blip direction must be positioned outside of the object [3]. Thus, a large distance of the side excitations (field-of-excitation, FOE) may be needed which requires long 2DRF pulses. In the second ("SE*"), a spin echo is generated and T2*-weighted acquisitions are obtained by shifting the central *k*-space line by an echo time offset TE_{GE} relative to the refocused spin echo (Fig. 1b). In this variant the 2DRF's line and blip directions are tilted by an angle φ such that the side excitations appear in the blind spot between the image slice and the slice stack to be acquired and are not refocused [6]. Thus, they can be positioned close to the main excitation which reduces the FOE and shortens the 2DRF pulse [6].

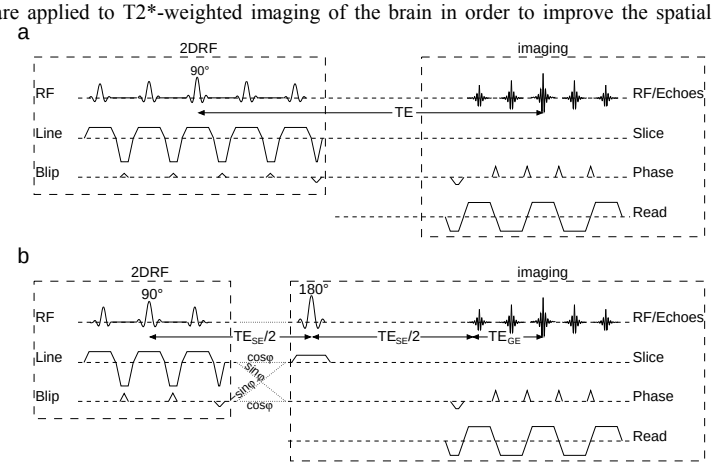

Fig. 1: Basic pulse sequences for T2*-weighted inner FOV imaging based on (a) the FID and a non-tilted setup (2DRF's blip is the phase encoding direction) and (b) a spin-echo signal with an echo time offset (TE_{GE}) and a tilted geometry to position side excitations outside of the image plane.

2DRF excitation (flip angle 90°) were based on a fly-back blipped-planar trajectory (see Fig. 1) with resolutions of 2.5×10 mm² (FID variant) and 5×10 mm² (SE* variant), respectively, and were designed under the low-flip-angle approximation [2]. For a FOV of 36 mm in the phase-encoding direction 18 mm oversampling were used to account for the profile transition regions (see Fig. 2). The FOE was 250 mm (25 k-space lines, 31.7 ms) for the FID variant and 70 mm (7 k-space lines, 6.6 ms) for the SE* variant with a tilt angle φ of 15°.

Measurements were performed on a 3T whole-body MR system (Siemens TIM Trio) using a 12-channel receive only-head coil. A water phantom and healthy volunteers from which informed consent was obtained prior to the examination, were investigated. Spatial resolutions between 2.0×2.0×5mm³ and 0.5×1.0×5mm³ were used. Functional neuroimaging was performed with a visual checkerboard stimulus (6 Hz, 12 blocks with 16.2s checkerboard and 16.2s gray screen) and a TR of 2.7s. Profile acquisitions were performed with a standard spin-echo sequence

Results

Profile acquisitions for the SE* variant demonstrate that the side excitations are reliably suppressed (Fig. 2) and do not interference with other slices of the stack (data not shown). The flat top of the SE* profile shows only minor signal variations (±5%) and no unwanted signal outside of the oversampled region. These results are also obtained for the FID variant (data not shown). Figure 3 shows the effect of a shim misadjustment on the 2DRF excitation profile which yields geometric distortions that are more pronounced for the FID variant due to its longer 2DRF pulse (31 ms vs. 7 ms). In Fig. 4, inner FOV images are compared to standard slice-selective acquisitions and demonstrate the reduced geometric distortions as well as the decreased signal dropout for FID acquisitions due to the shorter echo time achievable with inner FOVs (37 ms vs. 64 ms for 1×1 mm²). Results of the fMRI experiment are shown in Fig. 5. The brain activation in the visual cortex is less pronounced for the SE* variant (data not shown).

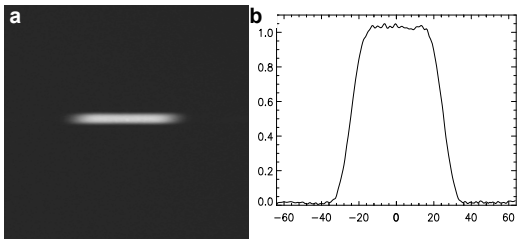

Fig. 2: Profile acquisition in a phantom (SE* variant): (a) MR image and (b) intensity plot along the FOV direction.

Fig. 3: 2DRF excitation profiles for an optimized shim (upper) and a shim misadjustment to simulate field inhomogeneities (lower) for the FID (left) and the SE* variant (right).

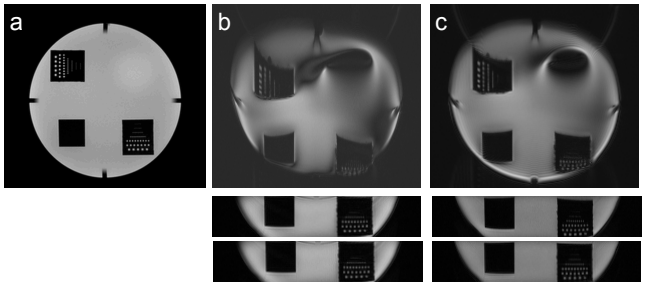

Fig. 4: (a) Localizer and (b,c) EPI acquisitions of a phantom with the (b) FID and the (c) SE* variant. The upper image was obtained with a standard slice-selective acquisitions (1×1mm²), the lower with inner-FOV imaging (1×1mm² and 0.5×1mm², respectively).

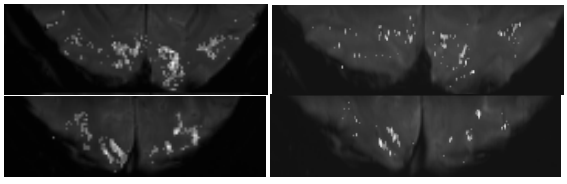

Fig. 5: Activation maps (two slices) of the visual checkerboard stimulus obtained with the FID variant overlaid on EPI images. The acquisitions were performed with a spatial resolution of 1×1mm² (left, TE 37 ms) and 0.5×1mm² (right, TE 46 ms).

Discussion and Conclusion

Due to the longer 2DRF pulse the minimum echo time for the FID variant may be quite long and the sensitivity of the excitation to field inhomogeneities is significant. In contrast, the SE* variant offers a flexible T2*-relevant echo time offset and reduced excitation profile distortions. However, brain activation was less significant for the SE* variant which to some extent is due to the more pronounced signal saturation for typical TR values used in fMRI experiments.

In conclusion, 2DRF excitation can be used to reduce geometric distortions in T2*-weighted imaging of small target volume. Thus, they may help to overcome spatial resolution limitations in functional neuroimaging.

References

[1] Bottomley PA, J. Appl. Phys. **62**, 4284 (1987)
[2] Pauly J, J. Magn. Reson. **81**, 43 (1989)
[3] Rieseberg S, Magn. Reson. Med. **47**, 1186 (2002)
[4] Saritas EU, Magn. Reson. Med. **60**, 1099 (2008)
[5] Finsterbusch J, J. Magn. Reson. Imaging **29**, 987 (2009)
[6] Finsterbusch J, ISMRM 19, 174 (2011)